Droplet Dynamics Changes in Electrostatic Sprays of Methanol−Water Mixtures

Zohra Olumee,[†] John H. Callahan,[‡] and Akos Vertes*[,†]

Department of Chemistry, The George Washington University, Washington D. C. 20052, and Analytical Chemistry Section, Code 6113, Naval Research Laboratory, Washington, D.C. 20375

Received: April 28, 1998; In Final Form: September 22, 1998

Two-dimensional phase Doppler anemometry measurements have been carried out to determine the size and velocity distributions of electrosprayed droplets generated from methanol−water mixtures. We investigated spraying conditions close to those of electrospray ionization sources. The droplet size and the axial and radial velocity distributions were measured as a function of liquid flow rate, needle-to-counter electrode distance, bias voltage, position of the probe volume, and electrical conductivity of the liquid. In 90:10 (v/v) methanol−water mixtures the droplet size decreased from ∼7 to ∼1.6 μm as the conductivity increased as a consequence of a 3 orders of magnitude increase in ionic strength. As the position of the probe volume was moved along the spray axis, two different spray dynamics were observed. Solutions of low conductivity ($c < 10^{-5}$ M) on the average produced 5.5 μm droplets at the capillary that gradually decreased to 4.0 μm as the drops moved away from the tip. Solutions of higher conductivity ($c > 10^{-3}$ M), however, resulted in smaller droplets at the needle (1.6 μm) that increased in size to 4.2 μm as the particles traveled toward the counter electrode. The droplet size reduction can be explained by evaporation and/or Coulomb explosion, whereas the increase in droplet size may be the consequence of droplet segregation or coalescence. Axial velocity distributions show compression along the spray axis (e.g., observed at 10 mm ∼50% reduction of the width at 4 mm is seen). Moving downstream, the average velocity of droplets from water−methanol mixtures decreases monotonically. Solutions containing KCl exhibit a maximum in axial droplet velocity as the probe volume moves away from the capillary. These profile changes can be explained by differences in the electric field distribution along the spray centerline.

Introduction

In the 1980s Fenn and co-workers initiated a highly successful application of electrostatic spraying as a source of ions for mass spectrometry.[1,2] They showed that using electrospray large and nonvolatile molecules can be ionized and transferred into the gas phase without degradation. This discovery revolutionized the mass spectrometry of biomolecules.[3,4]

In the electrospray source, solute ionization is achieved by applying high voltage to a metal capillary through which a slow flow of the solution is maintained. The potential gradient between the tip of the capillary and a counter electrode leads to the deformation of the meniscus and to the emission of charged liquid fragments that often take the form of spherical droplets. Depending on the physical properties of the liquid (electric conductivity, dielectric constant, surface tension, viscosity, and density) and on the spraying conditions (field strength at the tip, internal diameter and wettability of the capillary, and liquid flow rate), a rich variety of spraying modes can be established. According to the phenomenological classification of Cloupeau and Prunet-Foch, five major spraying modes can be distinguished (dripping, cone jet, microdripping, jet, and spindle modes).[5,6] This picture is substantially colored by variants of these modes (e.g., pulsed cone jet, multicone jet, ramified jet) and by the occurrence of corona discharge at elevated voltages.

Systematic investigations on the dispersion of liquids into small charged droplets by an electrostatic field originated more than a century ago when Rayleigh noticed that electrified droplets became unstable and underwent fission.[7] On the basis of Rayleigh's early results describing an isolated droplet, Zeleny also calculated the criteria for its stability.[7,8] They found that the potential at which instability began was proportional to the square root of the liquid surface tension.

Hendricks and co-workers proposed a somewhat arbitrary mathematical model that related the solution properties, such as surface tension, density, and conductivity, to the size and charge of a droplet.[9−12] This group varied the solution conductivity, the flow rate, and the field strength and measured the specific charge (charge-to-mass ratio) of the sprayed droplets. Both their theoretical and empirical models suggested that an increase in solution conductivity and in field strength or a decrease in flow rate leads to an increase in the specific charge according to a power law.[12]

Tang and Gomez reported results on atmospheric-pressure size, charge, and velocity distributions of heptane and deionized water[13−15] obtained by two optical diagnostic techniques: phase Doppler anemometry (PDA) and flash shadowgraphy. They provided clear photographic evidence of the Coulomb fission process of charged droplets under intense electric field stress.[13] It was found that the droplet charge-to-volume ratio was monotonically decreasing with increasing droplet size. According to their observations, larger droplets were closer to the limiting charge at which they underwent fission.[13]

Recently, the charge and size distributions of electrosprayed drops have been studied by Fernandez de la Mora and

* Corresponding author. Phone (202) 994-2717, Fax (202) 994-5873, E-mail vertes@gwu.edu.
[†] The George Washington University.
[‡] Naval Research Laboratory.

10.1021/jp982027z CCC: $15.00
Published on Web 10/28/1998

TABLE 1: Comparative Chart of Some Electrospray Characterization Studies

measured properties	spraying mode	spraying conditions[a]	methods	ref
charge and size distributions	cone jet	dibutyl sebacate and benzyl alcohol i.d. = 200 μm, U = "several kV"	differential mobility analyzer aerodynamic size spectrometer	16
specific charge	not reported	glycerin with NaCl i.d. = 500 μm, U < 30 kV	time-of-flight spectrometer	12
size distribution, specific charge	cone jet	water with NaCl at 10 kV < U < 20 kV	PDA	14, 18
	corona-assisted cone jet	heptane at U = "few kV", i.d. = 120 μm	flash shadowgraphy	15
spray current		1-octanol, water, benzyl alcohol, ethylene glycol, triethylene glycol, formamide with LiCl or H_2SO_4	current measurement	19
ion current	dripping cone jet multicone jet	water, CH_3OH, CH_3CN, water + CH_3OH (50:50) with LiCl or NaCl i.d. = 100 μm, 2.4 kV < U < 9.4 kV	mass spectrometer	1
ion current	not specified	water + CH_3OH with NaCl or HCl i.d. = 100 μm, 2 kV < U < 3 kV	mass spectrometer	21, 22
ion current, spray current	cone jet nanospray	acetone with rhodamine G i.d. = 250 μm at 2.5 kV < U < 3.6 kV i.d. = 1−3 μm at U = 600 V	mass spectrometer, microscope	23
spray current	pulsating cone jet cone jet	water + CH_3OH (50:50) 2.2 kV < U < 4.0 kV	current measurement, microscope	20

[a] i.d. and U denote the internal diameter and the voltage of the capillary, respectively.

co-workers utilizing a differential mobility analyzer and an aerodynamic size spectrometer.[16,17] The sprayed drops were selected within a narrow electrical mobility range, and subsequently the associated current or size was measured. Their findings indicated that the charge distribution of electrospray drops generated in cone-jet mode was 2.5 times broader than the corresponding distribution of diameter. They related the random process of jet breakup to the wavelength of axial modulation of the jet.[16]

The complexity of spraying modes made the electrospray phenomenon an elusive target for rigorous investigations and seriously limited the ability to compare results from different laboratories. Table 1 lists the measured spray properties and spraying conditions in some recent studies. It is clear from comparing the fundamental studies of the spraying process (first three rows of Table 1) with the studies on electrospray ionization (ESI) sources for mass spectrometry (rows four to seven of Table 1) that there is very limited overlap between these groups in spraying conditions. While well-controlled sprays were characterized in detail using powerful spray diagnostics,[12,14−16,18,19] the sprays typically used in ESI are mostly studied by following the generated ion current or the capillary current.[1,20−23] More specifically, there is no detailed droplet size diagnostics available for the very important case of methanol−water mixtures sprayed at relatively low voltages (2.0 kV < U < 5.0 kV).

Studying the capillary current as a function of capillary potential in 50:50 methanol−water mixtures, Rollgen and co-workers established three spraying modes based on the presence and frequency of current oscillations.[20] Mode I (2.2 kV < U < 2.5 kV) and mode II (2.5 kV < U < 2.8 kV) are characterized by 30 Hz and low kilohertz current pulsation, respectively. In mode III (2.8 kV < U < 4.0 kV) no current pulsation occurs. Optical investigation of the meniscus revealed that modes I and II corresponded to the pulsed cone-jet mode, whereas mode III coincided with the cone-jet mode.

The formation of charged droplets and their fate in the spray are the basis of ion production in an ESI source. In ESI sources used in mass spectrometry, the solution properties can change dramatically from one sample to the other. For example, the ionic strength and thus the conductivity of the sprayed solution change significantly with the salt content of the sample. Thus,

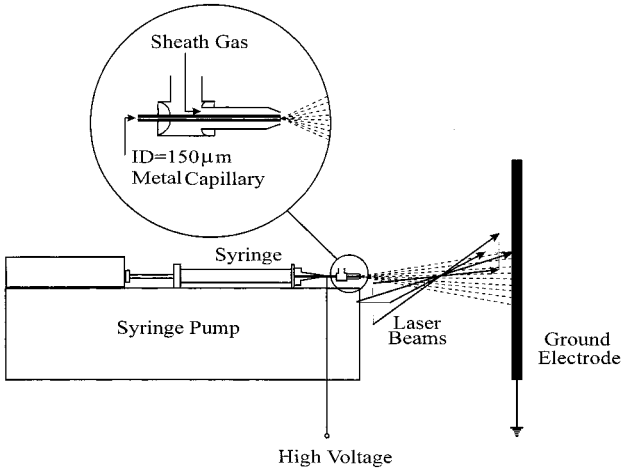

Figure 1. Constant flow-rate electrospray setup consisting of a syringe pump, syringe, stainless steel capillary, and planar ground electrode. Intersection of the PDA laser beams marks the probe volume.

the main objective of our present study was to obtain droplet size and velocity distributions for sprayed solutions typical of ESI under a broad range of spraying conditions. We also wanted to characterize the generated droplets as a function of fluid delivery system and liquid properties such as liquid flow rate, bias voltage, position of the probe volume, and electrical conductivity.

Experimental Section

The schematic representation of the electrospray setup is shown in Figure 1. A steady flow of the sprayed liquid was fed by a syringe pump (Sage Instruments, Boston, MA) into an i.d. = 150 μm and o.d. = 510 μm stainless steel capillary. To facilitate the desolvation of the droplets and to prevent electric breakdown, the capillary was surrounded by a tapered glass tube that provided a coaxial flow of dry nitrogen (see inset in Figure 1). The flow rate of the gas was selected by a needle valve and kept constant throughout the measurements. An X-Y-Z stage afforded the translation of the syringe pump and the

spraying assembly with an accuracy of 0.5 mm. Perpendicular to the capillary, a flat ground electrode was positioned at a distance of 30−35 mm. Stable spraying was achieved by applying high voltage (3.0−4.8 kV) to the needle. These values were similar to the ones used in ESI sources for mass spectrometry.[21,22] Lowering the voltage to 2−3 kV invariably resulted in pulsating sprays. Most of the systematic studies were conducted at $U = 4.0$ kV capillary voltage. The flow rate of the liquid was maintained at 24 μL/min, which was typical of ESI systems[21,22] but significantly higher than the values in some of the fundamental investigations.[16] As shown in Figure 1, the probe volume was defined by the intersection of four laser beams.

A two-color PDA system (Aerometrics, Sunnyvale, CA) was used to simultaneously sample the size and the axial and radial velocity distributions of the electrospray-generated droplets. The scattered light from the particle traveling through the probe volume was picked up by a receiving lens of 250 mm focal length positioned at 30° angle in forward scattering mode. The size of the probe volume depends on the collection angle and on the focal length of the focusing lens. Using a 250 mm focal length lens and a 100 μm slit resulted in 200 μm width for the probe volume. As has been pointed out by Sankar et al., a receiving lens with short focal length improves both the accuracy and the resolution in the measurements of small sized droplets.[24] Since the transmitter and receiver were positioned on opposite sides of the flow, system alignment was crucial and difficult to maintain. However, this orientation offered the best overall performance, high S/N, and excellent size sensitivity for the PDA system. The scattered light was projected onto three photomultiplier tubes (A, B, and C). Each detector produced a Doppler burst signal with a frequency proportional to the particle velocity. The phase shifts between the Doppler burst signals from the different detectors were proportional to the size of the spherical particles. Scattering obtained from nonspherical particles was rejected via a validation method based on comparing phase shifts on different pairs of detectors (e.g., A−B with B−C). If the phase shift difference exceeded 5%, the reading was discarded by the signal-processing unit.

Special care was taken to minimize the effect of scattering by multiple particles. Regular direct observation of the Doppler burst signal on an oscilloscope (TDS 320, Tektronix, Beaverton, OR) provided evidence that the probe volume was small enough to avoid significant contribution to the scattering signal by more than one particle. Temporal variations in the spray conditions were monitored by repeating the PDA measurements at different stages after establishing stationary spray conditions. No significant variations were detected. Simultaneous size and velocity measurements on the same droplet confirmed that there was no size-dependent segregation between the droplets in terms of their velocities (see details in the Results and Discussion section).

Analytical reagent grade methanol (<0.07% in H_2O) and deionized water (18.0 Mmho/cm) were used as spraying solutions in a 50:50 or 90:10 (v/v) mixing ratio. Only the results on the 90:10 systems are presented in this report. Reagent grade KCl (Fisher, Springfield, NJ) solutions of 5.0×10^{-3}, 5.0×10^{-4}, 5.0×10^{-5}, and 5.0×10^{-6} M concentration were prepared in the methanol−water mixture.

Results and Discussion

To probe the droplet behavior between the capillary and the ground electrode, we measured the size, the axial, and the radial velocity distributions when moving the probe volume along the spray axis. Spraying 90% methanol at 4.0 kV resulted in broad size distributions extending beyond 15 μm close to the capillary tip (see dashed line in Figure 2). Moving the probe volume from 4 to 10 mm resulted in compression of the distribution with the mean diameter changing from 6.9 to 4.8 μm. No significant change in the average droplet size was observed as measurements were made further down the spray axis, but on occasion the distribution became bimodal. Increasing the conductivity of the solution led to dramatic changes in both the droplet size distribution and its behavior along the spray axis. The solid lines in Figure 2 show the distributions that belong to 90:10 methanol−water mixtures doped with 5.0×10^{-3} M KCl. At $d_{pr} = 4$ mm probe volume−capillary tip distance the average droplet size, D_{10}, changed from 6.9 to 1.5 μm, whereas the fwhm of the distribution was compressed from 10.2 to 1.0 μm. In the case of high-conductivity solutions, moving away from the capillary tip resulted in an increase of the average diameter (e.g., from $D_{10} = 1.5$ μm at $d_{pr} = 4$ mm to $D_{10} = 3.9$ μm at $d_{pr} = 22$ mm). This trend was the opposite of what was observed for 90% methanol without a solute. It also contradicted the general assumption that droplets shrink in size along their trajectories due to evaporation and/or fission caused by instabilities.

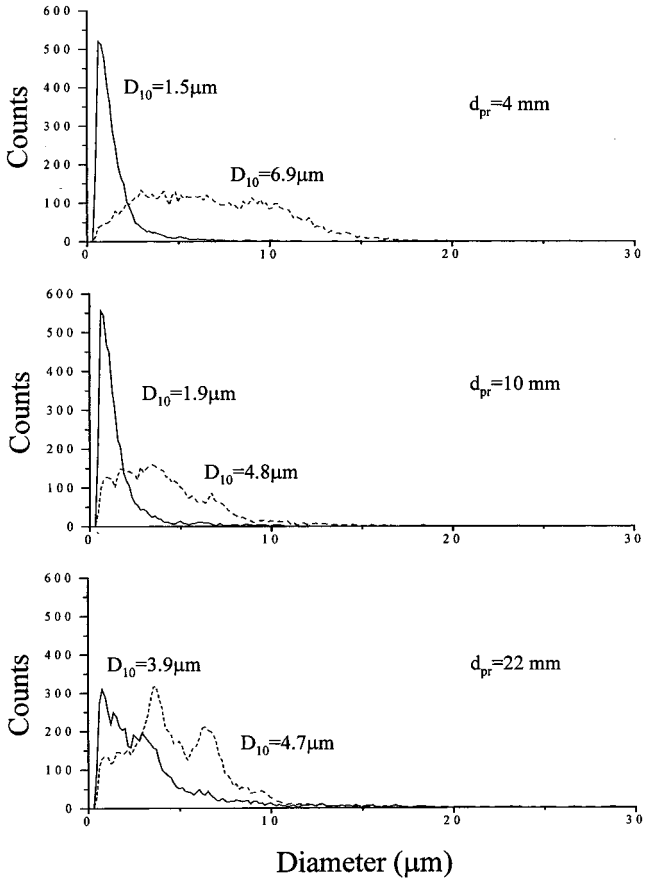

Figure 2. Size distributions of electrosprayed droplets from a 90:10 methanol−water mixture (dashed line) and the same mixture doped with 5.0×10^{-3} M KCl (solid line) as a function of the probe volume-to-capillary tip distance (d_{pr}). Stable spray was maintained at $U = 4.0$ kV capillary voltage.

To further investigate this phenomenon, a series of KCl solutions were prepared in 90% methanol with solute concentrations varying from 5.0×10^{-6} to 5.0×10^{-3} M. The average droplet diameter changes along the spray axis for the four different solutions, and the solvent are shown in Figure 3. While increasing the KCl concentration led to a significant decrease

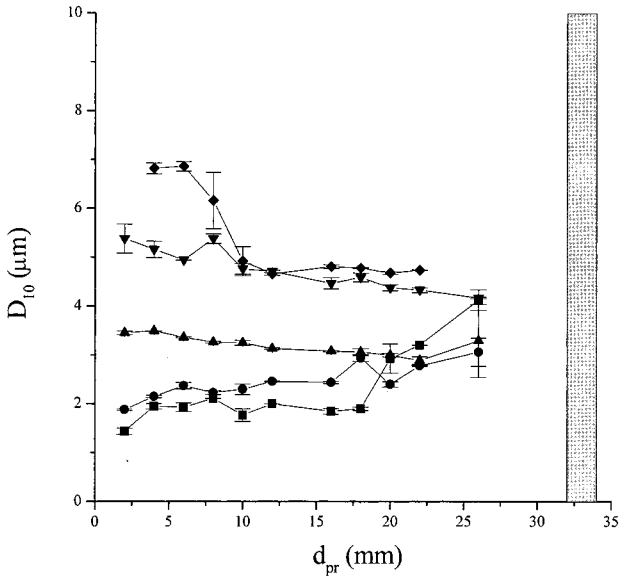

Figure 3. Effect of conductivity (ionic strength) on the average droplet diameter, D_{10}, probe volume position, d_{pr}, relationship. Ionic strength of a 90:10 methanol−water mixture was adjusted by addition of KCl (◆, no KCl; ▼, 5.0×10^{-6} M; ▲, 5.0×10^{-5} M; ●, 5.0×10^{-4} M; ■, 5.0×10^{-3} M KCl). The grayed box on the right shows the cross section of the ground electrode.

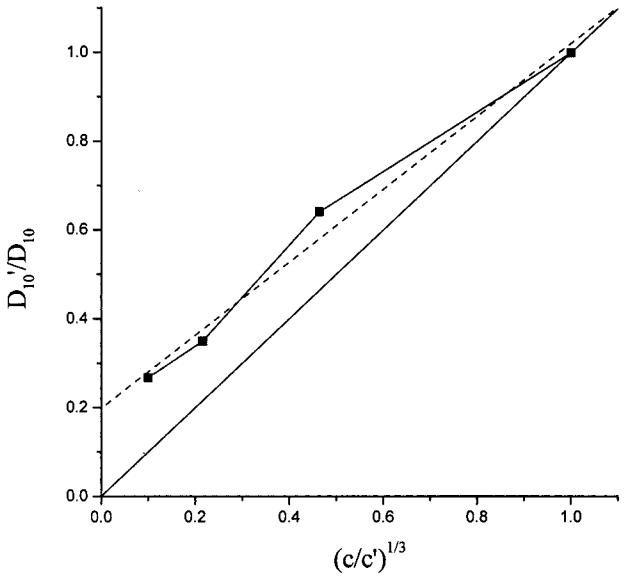

Figure 4. Variation of relative droplet diameter with the inverse of the relative concentration for electrosprayed dilute KCl solutions. The solid line represents eq 4, whereas the dashed line is a linear fit to the experimental data ($R = 0.99$).

in the initial droplet size, the observed variations at larger probe volume distance showed different trends for low-conductivity (no salt, 5.0×10^{-6} and 5.0×10^{-5} M) and for high-conductivity (5.0×10^{-4} and 5.0×10^{-3} M) solutions. In agreement with our preliminary observations, increasing the measurement distance from the capillary led to a decrease in droplet size for low-conductivity solutions, whereas high conductivity resulted in an increase in droplet size with distance.

To compare our results on the conductivity dependence of the average diameter with previous studies, we used the scaling law introduced by Fernandez de la Mora for solutions with electrical conductivities $\kappa > 10^{-7}$ Ω^{-1} cm^{-1}.[16] For a variety of conditions the droplet diameter, D, can be approximated as

$$D = G(\epsilon,\Pi_\mu)\left(\frac{\epsilon\epsilon_0 Q}{\kappa}\right)^{1/3} \tag{1}$$

where Q and κ are the flow rate and the electrical conductivity of the liquid, respectively. $G(\epsilon,\Pi_\mu)$ is a slowly varying function of the dielectric constant, ϵ, and the viscosity variable, Π_μ. It is assumed in the derivation of eq 1 that the liquid is conductive enough so that the diameter of the jet is much smaller than the i.d. of the needle. In addition, the liquid has to satisfy specific conditions on polarity or viscosity.[16] Since (1) has also been verified on deionized water,[14] the solutions used in the present study also satisfy the conditions for validity. For strong electrolytes κ can be written as

$$\kappa = (\Lambda^0_m - K\sqrt{c})c \tag{2}$$

where Λ^0_m is the molar conductivity at infinite dilution and K is the Kohlrausch constant. Assuming that for dilute solutions the variations in dielectric constant and viscosity are negligible and keeping the flow rate constant, the concentration dependence of the average droplet diameter is expressed as

$$\frac{D'}{D} = \left(\frac{c}{c'}\right)^{1/3}\left(\frac{\Lambda^0_m - K\sqrt{c}}{\Lambda^0_m - K\sqrt{c'}}\right)^{1/3} \tag{3}$$

where D' is the average droplet diameter at c' concentration. For the lowest KCl concentration in this study $c = 5.0 \times 10^{-6}$ M and $\Lambda_m = 104$ Ω^{-1} cm^2 mol^{-1} for the methanol-based solutions;[25] thus, $\kappa = 5.2 \times 10^{-7}$ Ω^{-1} cm^2 and eq 1 applies. In the concentration range of our interest variations in the molar conductivity of KCl are less than 6%; therefore, eq 3 simplifies to

$$\frac{D'}{D} \approx \left(\frac{c}{c'}\right)^{1/3} \tag{4}$$

Figure 4 shows the measured relative diameter as a function of relative concentration at $d_{pr} = 2$ mm probe volume position for KCl solutions spanning 4 orders of magnitude in concentration. The solid straight line with a slope of one in Figure 4 corresponds to eq 4. Although there was clear deviation from eq 4 at elevated concentrations, a linear fit of the data points yielded a slope of 0.82 and a regression coefficient of 0.99. Some of the assumptions, most notably about the concentration-independent nature of $G(\epsilon,\Pi_\mu)$, are likely to break down at high salt content and may cause the discrepancies observed in Figure 4.

Shrinking droplet size with increasing distance from the spraying tip has been observed repeatedly for high vapor pressure liquids such as heptane[13,18] and for deionized water.[14] The droplet size reduction in these systems is initiated by evaporation. Further dispersion of the liquid takes place as a consequence of Coulomb fission leading to smaller droplets. The driving force behind Coulomb fission is that the evaporation increases the charge-to-mass ratio of the droplets leading to surface instabilities and eventually to their rupture. On the basis of this physical picture, we had no difficulty explaining the results observed on low-conductivity liquids. It is not feasible, however, to explain the observed average droplet size *increase* in high-conductivity systems with the fission mechanism.

The most plausible explanation for the apparent growth in the observed droplet size is a fractionation effect. Cone-jet type sprays are known to have two major directional components. The first one is composed of the larger *primary droplets* traveling close to the spray axis leaving under a small solid angle. The second component is the "skirt" of the spray made of smaller *satellite droplets* departing under a larger solid

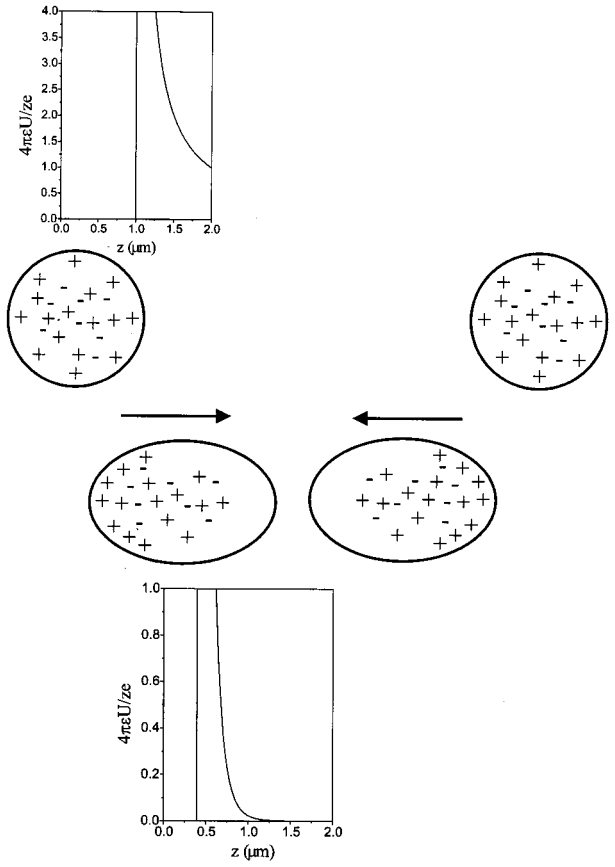

Figure 5. Charge and potential distributions in two homopolar droplets at large distance (top) and at close proximity (bottom). As the droplets approach each other, excess charges congregate at the opposite ends of the spheroids, and due to the presence of the electrolyte shielding takes place. Depending on the conductivity (ionic strength), shielding may be sufficient to minimize electrostatic repulsion and promote coalescence.

angle.[13] As the spray diverges along its axis, the two components increasingly segregate.[16] While the smaller satellite droplets move off axis, the larger primary droplets remain close to the center. This process leads to the enrichment of the sampled downstream axis locations in larger droplets. Increasing segregation with increasing conductivity can be explained by assuming enhanced space-charge repulsion due to the formation of smaller highly charged droplets.

Another possible interpretation of the growing droplet size is the increasing incidence of droplet coalescence at higher conductivities, i.e., higher ionic strengths. Given the substantial amount of charges associated with the droplets, their collision and coalescence are considered unlikely even at large particle densities. There are two factors, however, that might help to explain the collision of homopolar droplets. The first one is their high kinetic energy. Based on the measured values of the average diameter ($\sim$2 μm) and the velocity ($\sim$10 m/s), the kinetic energy of a single droplet is $E_{kin} \approx 2 \times 10^{-6}$ erg or $\sim 10^6$ eV. More importantly, when two droplets of similar charge approach each other, they undergo deformation and charge rearrangement (see Figure 5). As the droplets approach each other, their shape changes from spherical to elongated spheroid, and the free charges originally located at the surface congregate at the opposite ends of the spheroid. Within the droplet the ions of the strong electrolyte rearrange, so as they modify the original Coulomb potential around the sphere into a shielded Coulomb potential with a shielding length that is inversely proportional to the square root of the ionic strength

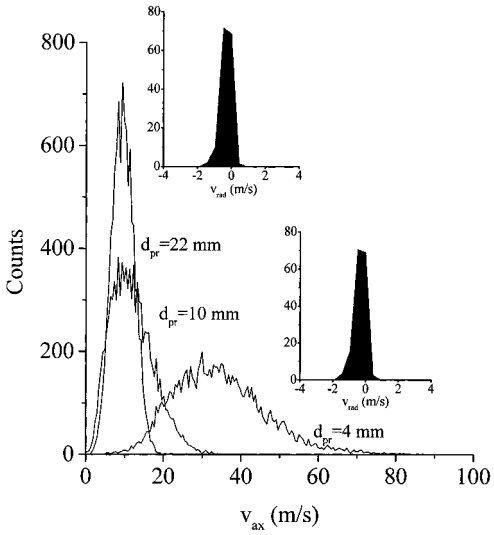

Figure 6. Axial velocity distribution of droplets electrosprayed from 90% CH_3OH at different probe volume positions, d_{pr}. Moving away from the capillary tip, the average velocity drops and the velocity spread is compressed. Corresponding radial velocity distributions are shown in the insets for $d_{pr} = 4$ mm and $d_{pr} = 22$ mm.

(see insets in Figure 5). Increasing the ionic strength shortens the shielding length and at sufficiently high conductivity; i.e., high electrolyte concentration may eliminate the repulsion between the two approaching droplets. For example, the shielding length, r_D, for a 5.0×10^{-6} M KCl aqueous solution is 140 nm, whereas at 5.0×10^{-3} M $r_D = 4$ nm. This sharp increase in shielding in combination with the charge rearrangement may lead to coalescence upon collision. We need to mention that—as was shown by Rayleigh and Taylor— too much deformation of a droplet leads to fission.[7,26] When the length of a droplet exceeds the equatorial diameter by a factor of 1.9, the droplet becomes unstable. Thus, collision of droplets can lead to coalescence, fission, or a combination of the two.

Axial and radial velocity distributions of droplets sprayed from 90% CH_3OH are shown in Figure 6. There was a remarkable variation in the axial velocity distributions as a function of probe volume position. When the measurements were conducted closer to the capillary tip (e.g., $d_{pr} = 4$ mm), broader distributions and larger mean velocities were observed. As the distance increased from $d_{pr} = 4$ to 10 and to 22 mm, the axial mean velocity decreased from 34.5 to 11.4 and to 9.6 m/s, respectively. At the same time, the width of the velocity distributions became significantly narrower. Comparing the distributions revealed that the fwhm at $d_{pr} = 10$ and 22 mm downstream were about one-half and one-third of the fwhm at $d_{pr} = 4$ mm, respectively. While slowing of the droplets can be a natural consequence of the interplay between the electric field and the drag force, the velocity compression can be rationalized by looking at the actual form of the latter. For flows with $Re < 1000$, the explanation can be based on the velocity-dependent nature of the corrected Stokes drag force, $\mathbf{F}_{dr}$:[18]

$$\mathbf{F}_{dr} = 3\pi\mu D(1 + 0.158Re^{2/3})(\mathbf{v} - \mathbf{v}_g) \qquad (5)$$

where μ is the viscosity of the medium, Re is the Reynolds number, and $\mathbf{v}$ and $\mathbf{v}_g$ are the velocities of the particle and the gas, respectively. Assuming that the velocity of the gas is constant in the region of interest, higher droplet velocity corresponds to higher decelerating force. Thus, the faster particles are slowed more efficiently than the slow ones leading to the bunching of velocities.

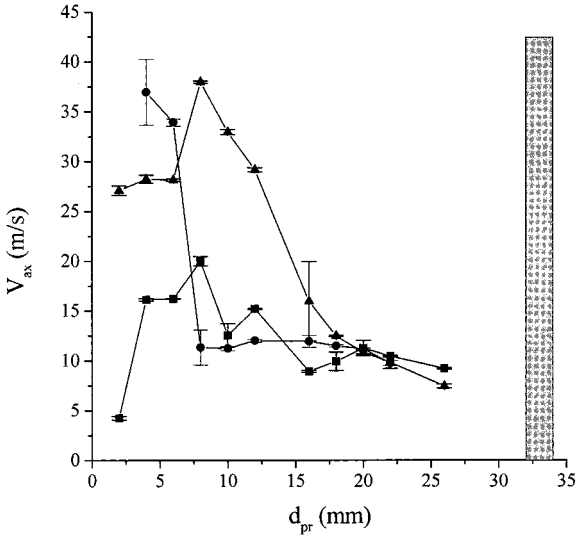

Figure 7. Probe volume position dependence of average axial velocity, v_{ax}, of droplets generated from a 90:10 methanol−water mixture (●) and from the same solvent doped with 5.0×10^{-6} M (▲) and with 5.0×10^{-3} M (■) KCl.

Radial velocity distributions are shown in the insets of Figure 6. These distributions were substantially narrower than their axial counterparts. They were centered around zero and showed no dependence on the probe volume position. This observation had some implications on the forces controlling the motion in the radial direction. Since the most significant forces acting on a droplet at these velocities are related to the external electric field, $\mathbf{E}_{ext}$, the electric field associated with space charge, $\mathbf{E}_{sc}$, and the drag force, one can write

$$\mathbf{F} = ze\mathbf{E}_{ext} + ze\mathbf{E}_{sc} - \mathbf{F}_{dr} \tag{6}$$

where z is the number of elementary charges, e, on the droplet. No change in the radial velocity distribution means that the ensemble average of the radial component of **F** is close to zero. Thus, in radial direction either the electrostatic forces balance out the drag force or all of them are negligible.

For three solutions of different conductivity, the probe volume position dependence of the average axial velocity is displayed in Figure 7. Observing the data at $d_{pr} = 2$ mm probe position indicated that increasing the conductivity led to lowering of the initial velocity. Indeed, the droplets from a 90:10 methanol−water mixture departed with an average velocity >37 m/s, whereas from 5.0×10^{-6} and 5.0×10^{-3} M KCl solutions they left with a speed of 27 and 4 m/s, respectively. One might conclude that this behavior—in combination with the observed shrinkage in initial droplet size with increasing conductivity—is related to the morphological changes of the cone-jet structure and to the profound differences in field penetration due to shielding.

Another interesting feature in Figure 7 is the difference in the position dependence of droplet velocities from different solutions. The droplets from pure solvent (90% methanol) exhibited monotonically decreasing average velocities with increasing distance from the probe tip, whereas the KCl solutions showed maximum velocity at a finite distance from the capillary. Tang and Gomez obtained the spray momentum equation on the centerline in the following form:

$$\overline{v_z}\frac{\partial \overline{v_z}}{\partial z} \cong \frac{1}{m}\overline{F_z} \tag{7}$$

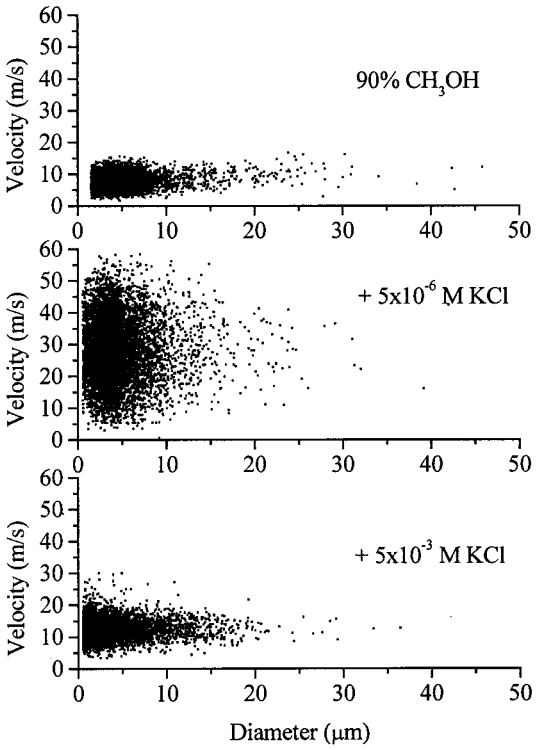

Figure 8. Velocity−size correlation of droplets electrosprayed from 90:10 CH_3OH−water mixture and from 5.0×10^{-5} and 5.0×10^{-3} M KCl solutions. In the lowest-conductivity case (no salt) there are some very large droplets, whereas in the high-conductivity case (5.0×10^{-3} M KCl) the velocity distribution is substantially broadened. As the conductivity increases, the size distribution compresses and the average velocity as well as its spread grows.

where the z subscript signifies the axial component of the velocity and the force determined by eqs 5 and 6. The overbar indicates average quantities defined using the $f(\mathbf{x},\mathbf{v})$ droplet distribution function; for example, the average velocity is calculated as $\bar{\mathbf{v}} \equiv (1/N)\int f(\mathbf{x},\mathbf{v})\mathbf{v}\, d\mathbf{v}$, where $N \equiv \int f(\mathbf{x},\mathbf{v})\, d\mathbf{v}$. Equation 7 is based on a number of specific assumptions regarding the spray (no source or sink terms, no evaporation effects, steady-state conditions, monodispersity, etc.). Some of these are clearly not fulfilled in our spray (changing droplet size, departure from monodispersity), and some others are not verified. Thus, quantitative evaluation of the results based on eq 7 is unfounded. Already in this simplified form, however, eq 7 shows a relationship between the position dependence of the axial velocity and the distribution of electric field. Assuming that there is no first-order effect by the conductivity on the drag force, one can argue that the significant changes in the shape of $v_{ax}(d_{pr})$ with conductivity are primarily due to changes in the space-charge component of the electric field. More specifically, one can assume that the accelerating effect on high-conductivity droplets near the capillary is the consequence of a sharper potential drop in that region corresponding to "shielding" by the high-ionic-strength droplets.

Axial velocity−size correlation charts for methanol−water mixtures at different salt content are shown in Figure 8. In this data acquisition mode velocity and diameter data are gathered on the same particle and rendered on a scatter chart. Statistical analysis of correlated measurements helps to find interdependence between variables and to detect segregation effects. The data were collected on the centerline, 10 mm away from the capillary tip where the accelerating effect of the electric field was negligible. One of the interesting features, observed with 90% methanol, is the presence of an extended tail in the

size distribution leading to some very large droplets ($D > 40$ μm). In accordance with Figures 3 and 7, at 5.0×10^{-6} M KCl concentration the center of the distribution shifts to smaller sizes and higher velocities. Somewhat unexpectedly, the spread of axial droplet velocities also increases significantly. At 5.0×10^{-3} M KCl concentration the center of the distribution shifted to smaller diameters, and the average velocity (as well as its spread) decreased.

It was worth noting that there was no correlation between size and velocity for any of the solutions. Similarly, no segregation of particles was observed. These findings support the mathematical decoupling of the droplet distribution function: $f(z,v_{ax}) = f_1(z)\, f_2(v_{ax})$. In other words, the size and velocity distributions measured separately can be combined to provide the droplet distribution function. It is known, however, that the radial component of the velocity shows correlation with the size of the particles.[18] The larger primary droplets exhibit lower radial velocities, whereas the smaller satellite droplets have higher radial velocity components. This effect leads to the segregation of the primary and satellite droplets under different solid angles. Although we measured radial droplet velocity distributions, the corresponding size−velocity correlations were not recorded. Moreover, due to the small size cutoff of our PDA system (0.5 μm), most of the satellite droplets probably went undetected.

Conclusions

Based on PDA, observations of ESI type sprays used in ion generation led to the recognition of significant changes in spray dynamics as the conductivity of the liquid was increased. As the conductivity grew within the boundaries of normal operating conditions, we detected a reversal in trend from shrinking average droplet size along the spray axis to a growing one. At the same time, the average axial velocity profile changed from a monotonic drop to maximum behavior. The sampling uniformity of these sprays improved downstream in terms of both their average diameter and axial velocity. For example, at 22 mm probe volume position v_{ax} was ~10 m/s independent of the velocity at the tip of the capillary and independent of the conductivity (Figure 7). Similarly, the D_{10} values converged as the droplets approached this region (Figure 3). This behavior has beneficial implications for the design of ESI sources. Prevailing source designs feature a comparable distance between the spraying needle and the sampling capillary. To rationalize the growing average droplet size in high-conductivity solutions, we offered two alternative explanations. One was based on size-dependent segregation along the spray axis, whereas the other evoked a coalescence model based on droplet−droplet polarization and internal shielding.

Acknowledgment. The authors thank the financial assistance of the National Science Foundation (CHE-9512441) for purchasing the PDA instrument. Z.O. is grateful for partial support by the George Washington University. Discussions with Keqi Tang of Finnigan Co. were valuable in providing alternative explanations for some of the data. The fabrication of the spraying assembly and helpful advice on its operation by M. Shahgholi are appreciated.

References and Notes

(1) Yamashita, M.; Fenn, J. B. *J. Phys. Chem.* **1984**, *88*, 4451−4459.
(2) Meng, C. K.; Mann, M.; Fenn, J. B. *J. Phys. D: At., Mol. Clusters* **1988**, *10*, 361−368.
(3) Fenn, J. B. *J. Am. Soc. Mass Spectrom.* **1993**, *4*, 524−535.
(4) Fenn, J. B.; Mann, M.; Meng, C. K.; Wong, S. F.; Whitehouse, C. M. *Mass Spectrom. Rev.* **1990**, *9*, 37−70.
(5) Cloupeau, M.; Prunet-Foch, B. *J. Aerosol Sci.* **1994**, *25*, 1021−1036.
(6) Cloupeau, M.; Prunet-Foch, B. *J. Electrost.* **1990**, *25*, 165−184.
(7) Rayleigh F. R. S. *Philos. Mag.* **1882**, *14*, 184−186.
(8) Zeleny, B. A. *Proc. Cambridge Philos. Soc.* **1916**, *18*, 71−83.
(9) Hendricks, C. D. *J. Colloid Interface Sci.* **1962**, *17*, 249−259.
(10) Hogan, J. J.; Hendricks, C. D. *AIAA J.* **1965**, *3*, 296−301.
(11) Swatik, D. S.; Hendricks, C. D. *AIAA J.* **1968**, *6*, 1596−1597.
(12) Pfeifer, R. J.; Hendricks, C. D. *AIAA J.* **1968**, *6*, 496−502.
(13) Gomez, A.; Tang, K. *Phys. Fluids* **1994**, *6*, 404−414.
(14) Tang, K.; Gomez, A. *J. Aerosol Sci.* **1994**, *25*, 1237−1249.
(15) Tang, K.; Gomez, A. *J. Colloid Interface Sci.* **1995**, *175*, 326−332.
(16) De Juan, L.; Fernandez de la Mora, J. *J. Colloid Interface Sci.* **1997**, *186*, 280−293.
(17) Loscertales, G.; Fernandez de la Mora, J. *J. Chem. Phys.* **1995**, *12*, 5041−5060.
(18) Tang, K.; Gomez, A. *Phys. Fluids* **1994**, *6*, 2317−2332.
(19) Fernandez de la Mora, J.; Loscertales, I. G. *Fluid Mech.* **1994**, *260*, 155−184.
(20) Juraschek, R.; Schmidt, A.; Karas, M.; Rollgen, F. W. In *Proceedings of the 45th ASMS Conference on Mass Spectrometry and Allied Topics*, Palm Springs, CA; ASMS: Santa Fe, NM, 1997; p 117.
(21) Kebarle, P.; Tang, L. *Anal. Chem.* **1993**, *65*, 972A−986A.
(22) Tang, L.; Kebarle, P. *Anal. Chem.* **1991**, *63*, 2709−2715.
(23) Wilm, M. S.; Mann, M. *Int. J. Mass Spectrom. Ion Processes* **1994**, *136*, 167−180.
(24) Sankar, S. V.; Weber, B. J.; Kamemoto, D. Y.; Bachalo, W. D. *Appl. Opt.* **1991**, *30*, 4914−4920.
(25) Kebarle, P.; Ho, Y. In *Electrospray Ionization Mass Spectrometry: fundamentals, instrumentation, and applications*; Cole, R. B., Ed.; John Wiley & Sons: New York, 1997; pp 3−63.
(26) Taylor, G. *Proc. R. Soc. London, Ser. A* **1964**, *280*, 383−397.